

RESEARCH ARTICLE

Ablation of oligodendrogenesis in adult mice alters brain microstructure and activity independently of behavioral deficits

Malte S. Kaller¹  | Alberto Lazari¹  | Yingshi Feng¹ | Annette van der Toorn² | Sebastian Rühling^{1,3} | Christopher W. Thomas⁴  | Takahiro Shimizu⁵  | David Bannerman⁶  | Vladyslav Vyazovskiy^{4,7,8}  | William D. Richardson⁵  | Cassandra Sampaio-Baptista^{1,9}  | Heidi Johansen-Berg¹ 

¹Wellcome Centre for Integrative Neuroimaging, FMRIB, Nuffield Department of Clinical Neurosciences, University of Oxford, Oxford, UK

²Biomedical MR Imaging and Spectroscopy Group, Center for Image Sciences, University Medical Center Utrecht & Utrecht University, Utrecht, The Netherlands

³Department of Diagnostic and Interventional Neuroradiology, School of Medicine, Klinikum rechts der Isar, Technical University of Munich, Munich, Germany

⁴Department of Physiology, Anatomy and Genetics, University of Oxford, Oxford, UK

⁵The Wolfson Institute for Biomedical Research, University College London, London, UK

⁶Department of Experimental Psychology, University of Oxford, Oxford, UK

⁷Sir Jules Thorn Sleep and Circadian Neuroscience Institute, University of Oxford, Oxford, UK

⁸The Kavli Institute for Nanoscience Discovery, University of Oxford, Oxford, UK

⁹School of Psychology and Neuroscience, University of Glasgow, Glasgow, UK

Correspondence

Malte S. Kaller, Wellcome Centre for Integrative Neuroimaging, FMRIB, Nuffield Department of Clinical Neurosciences, University of Oxford, Oxford, UK.
Email: malte.kaller@ndcn.ox.ac.uk

Funding information

Wellcome Trust, Grant/Award Numbers: 102393/Z/13/Z, 110027/Z/15/Z, 203139/Z/16/Z, 203139/A/16/Z

Abstract

Oligodendrocytes continue to differentiate from their precursor cells even in adulthood, a process that can be modulated by neuronal activity and experience. Previous work has indicated that conditional ablation of oligodendrogenesis in adult mice leads to learning and memory deficits in a range of behavioral tasks. The current study replicated and re-evaluated evidence for a role of oligodendrogenesis in motor learning, using a complex running wheel task. Further, we found that ablating oligodendrogenesis alters brain microstructure (ex vivo MRI) and brain activity (in vivo EEG) independent of experience with the task. This suggests a role for adult oligodendrocyte formation in the maintenance of brain function and indicates that task-independent changes due to oligodendrogenesis ablation need to be considered when interpreting learning and memory deficits in this model.

KEYWORDS

EEG, motor learning, myelin, *Myrf*, oligodendrocytes, plasticity, preclinical MRI

Cassandra Sampaio-Baptista and Heidi Johansen-Berg contributed equally.

This is an open access article under the terms of the [Creative Commons Attribution](https://creativecommons.org/licenses/by/4.0/) License, which permits use, distribution and reproduction in any medium, provided the original work is properly cited.

© 2024 The Author(s). GLIA published by Wiley Periodicals LLC.

1 | INTRODUCTION

Myelination of axons plays a critical role in the functioning of the vertebrate nervous system by increasing the transmission speed and energy efficiency of neural processing (Nave, 2010; Salzer & Zalc, 2016). Recent studies have demonstrated that myelin is more dynamic than initially thought. Myelination can be stimulated by artificially exciting neuronal activity (Cullen et al., 2021; Gibson et al., 2014; Mitew et al., 2018), indicating that myelin plasticity, in addition to synaptic modification, might be one way in which experience can shape brain structure and function (Bonetto et al., 2021; Kaller et al., 2017; Xin & Chan, 2020). Indeed, changes in myelination and white matter (WM) microstructure have been consistently associated with learning in humans (Lakhani et al., 2016; Scholz et al., 2009) and rodents (Bacmeister et al., 2022; Sampaio-Baptista et al., 2013). In addition, adaptive myelination is proposed to regulate homeostatic coordination and oscillatory self-organization in local and large-scale brain networks (Dubey et al., 2022; Noori et al., 2020; Pajevic et al., 2014; Pajevic et al., 2023; Talidou et al., 2022). Thus, deficient myelin plasticity might lead to alterations in myelination and neural network function that impair neurological function (Geraghty et al., 2019; Knowles et al., 2022). Yet, the questions of when, how, and to what extent adaptive myelination contributes to relevant changes in neural circuit function require further investigation.

The formation of new oligodendrocytes (OLs), a process referred to as oligodendrogenesis, can adaptively shape myelination in the central nervous system (Bergles & Richardson, 2016; Foster et al., 2019). Mature OLs, the myelin forming glial cells, continue to differentiate even in adulthood (Hill et al., 2018; Hughes et al., 2018; Rivers et al., 2008; Young et al., 2013) from populations of oligodendrocyte precursor cells (OPCs) that remain abundant, dynamic and widespread in the CNS throughout life (Dawson et al., 2003). Recently, multiphoton imaging studies in live behaving mice have demonstrated continuous formation of OLs and changes in oligodendroglial cells dynamics in response to motor learning (Bacmeister et al., 2022; Hill et al., 2018; Hughes et al., 2018). However, the contribution of such continuous and adaptive oligodendrocyte lineage dynamics to the functioning of the nervous system is still not well understood.

Transgenic mouse lines that allow conditional ablation of oligodendrogenesis in early adulthood have provided information about the causal involvement of new oligodendrocyte formation in behavior. The first use of this transgenic approach revealed that mice with ablated oligodendrogenesis have an impaired ability to learn to run at speed on a complex wheel (CW), suggesting a deficit in motor skill learning (McKenzie et al., 2014; Xiao et al., 2016). Subsequent studies found that interrupting OL generation also leads to deficits in long-term consolidation of spatial and fearful memories (Pan et al., 2020; Steadman et al., 2020). Additionally, impaired training-induced improvements in spatial working memory have also been reported (Shimizu et al., 2023). However, if and how the disruption of oligodendrogenesis in adulthood affects the CNS, independent of experience in a specific task, remains understudied.

The current study set out to further probe our understanding of behavioral, anatomical and physiological consequences of disrupting the formation of new OLs during adulthood. Our primary aim at the onset was to study how genetic ablation of OL differentiation affects brain microstructure and activity in adult mice in the presence or absence of learning a new motor task. The secondary aim of the study was to replicate key findings indicating a motor learning deficit in adult mice with ablated oligodendrogenesis on the CW task (McKenzie et al., 2014; Xiao et al., 2016), which was used as the main behavioral test in this study. We hypothesized that disruption of new oligodendrocyte formation alters metrics of brain microstructure sensitive to myelin and, consequently, might modify cortical network activity. Further, we hypothesized that learning to run the CW will lead to changes in myelin-related metrics, which will be absent or altered in animals with disrupted oligodendrocyte formation. Our results indeed replicated the finding that ability to perform a CW running task is perturbed within the first hours of testing in animals with disrupted oligodendrogenesis. However, to run the CW did not lead to detectable changes in myelin-sensitive metrics of brain microstructure. Instead, disrupting oligodendrogenesis led to alterations in both the microstructure and activity of the brain, irrespective of animal's experience with the CW task.

2 | RESULTS

2.1 | Deleting *Myrf* in OPCs leads to ablation of oligodendrogenesis

In the current study, we used a transgenic mouse model that allowed conditional deletion of myelin regulatory factor (*Myrf*) in the resident PDGFR α -positive OPC population (*Pdgfra*-CreER^{T2}:R26R-YFP:*Myrf*^{fl/fl}); referred to as “P-*Myrf*” from here on (McKenzie et al., 2014). As *Myrf* encodes a transcription factor required for oligodendrocyte differentiation (Emery et al., 2009), animals with both alleles of *Myrf* conditionally deleted during adulthood (P-*Myrf*^{fl/fl}) have markedly reduced formation of new OLs 6 weeks after tamoxifen treatment (Figure 1), as compared with control animals with one functional allele (P-*Myrf*^{+/fl}).

2.2 | Ablation of oligodendrogenesis leads to impaired performance on the CW

Previous work has indicated that such conditional ablation of oligodendrogenesis in adult mice leads to learning deficits in a range of different behavioral tasks (McKenzie et al., 2014; Pan et al., 2020; Steadman et al., 2020). We aimed to re-examine the ability of such mice to learn to run on a complex running wheel with irregularly spaced rungs (McKenzie et al., 2014; Xiao et al., 2016) (Illustrated in Figure 2a).

A total of 124 animals (P-*Myrf*^{+/fl}; $n = 59$, 28 females; P-*Myrf*^{fl/fl}; $n = 65$, 29 females) were tested on the CW across

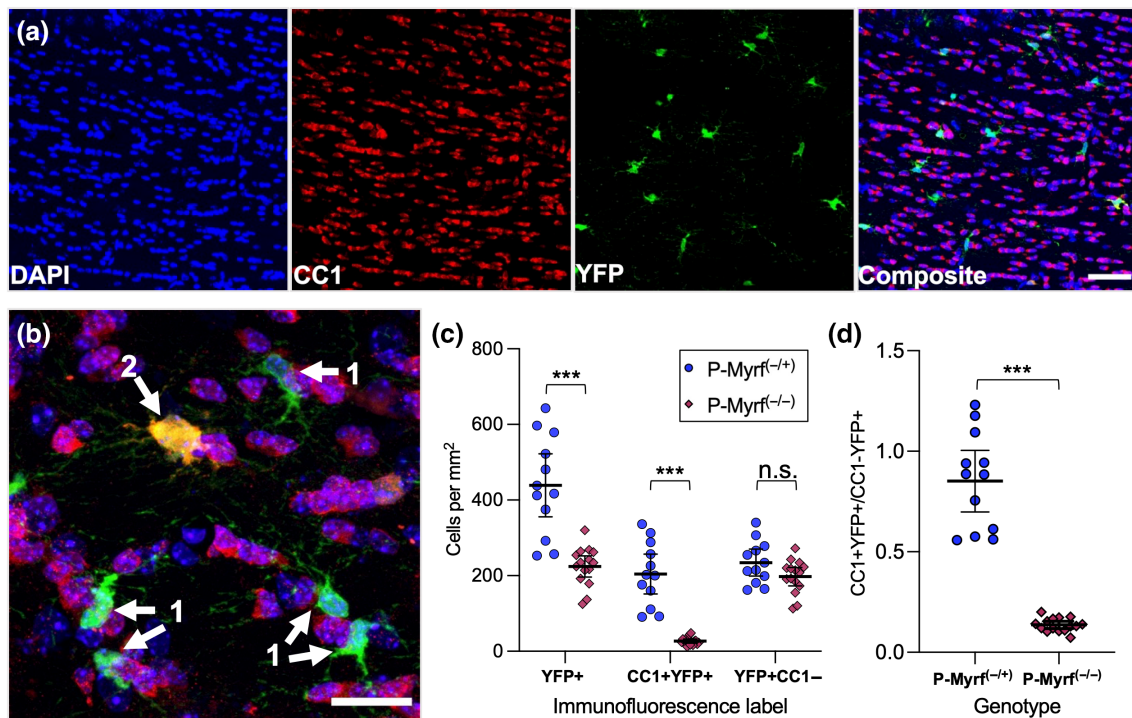


FIGURE 1 Deleting *Myrf* in oligodendrocyte precursor cells (OPCs) significantly reduced the formation of new oligodendrocytes (OLs). (a) Representative individual image of immunohistochemistry, split into its separate channels. DAPI was used to identify individual cell nuclei, CC1 was used to label mature OLs, and YFP marked OPCs at the time of tamoxifen administration (scale bar 50 μ m). (b) CC1+ and YFP+ cells were quantified and labeled as either (1) an OPC that remained YFP + |CC1-, or (2) a recently matured oligodendrocyte that was YFP + |CC1+. (c) Quantification confirmed a significant reduction of the density of YFP + |CC1+ recently matured OLs in the P-Myrf^{-/-} animals 6 weeks after tamoxifen administration. (d) The ratio between recently matured OLs (YFP + |CC1+) and labeled OPCs (YFP + |CC1-) was significantly lower in the P-Myrf^{-/-}. Data presented as Mean \pm 95%CI, Welch's two sample t-test used for statistical comparison. *** Represents statistical significance of $p < .001$. P-Myrf^{+/+}, $n = 12$; P-Myrf^{-/-}, $n = 15$.

several experiments (see Method section; Table S1). Animals received tamoxifen in early adulthood (age range: P60–90) and behavioral performance was tested 3–6 weeks later (Figure 2c).

To investigate whether ablation of *Myrf* in OPCs during adulthood impacts performance on the complex running wheel, we tested for main effects of genotype, time, and interactions on daily average and maximum speed using mixed two-way Analysis of Variance (ANOVA). Sex was included as an additional between-subject factor. Table S2 contains comprehensive information on the statistical analysis methods utilized and the corresponding results for each dataset.

A main effect of genotype for average speed ($F(1, 120) = 10.00$, $p = .002$, Figure 2d) and maximum speed ($F(1, 120) = 11.92$, $p < .001$, Figure 2e) over 8 days confirmed that overall performance metrics of P-Myrf^{-/-} animals were significantly lower than for their P-Myrf^{+/+} siblings. Furthermore, P-Myrf^{-/-} animals had impaired capacity to improve their performance with practice over training days mixed two-way ANOVA, time \times genotype interaction for average daily speed ($F(2.74, 328.5) = 5.56$, $p = .001$, Figure 2d) and maximum daily speed ($F(2.57, 308.9) = 4.76$, $p = .005$, Figure 2e). Females outperformed males in terms of running performance main effect of sex, average speed: $F(1, 120) = 13.1$, $p < .001$, maximum speed: $F(1, 120) = 17.5$, $p < .001$; (Figure S1g) and spent more time on the complex

running wheel (Figure S1h; Mann-Whitney U , $p = .014$), yet no statistically significant interaction between animals' sex and genotype was detected in any ANOVA test presented. Running ability on a normal running wheel and general motor skills, as tested by RotaRod and balance beam, were not impaired in the P-Myrf^{-/-} animals (Figure S1a–f), indicating that performance differences between genotypes did not generalize to other running tasks or tests of motor skill.

The average running speed (Figure 2f) and maximum running speed (Figure 2g) across the 8 days of training was lower in P-Myrf^{-/-} (Mann-Whitney U : average speed, Figure 2f, $p = .003$; maximum speed, Figure 2g, $p = .002$), further indicating a deficit in performance on the CW in animals with ablation of *Myrf* in OPCs during adulthood. However, the distribution of performance values was not equal between genotype groups, with higher variability and a bimodally shaped distribution especially prominent in the group of P-Myrf^{-/-} animals (Figure 2f,g), a feature that was also reported by McKenzie et al. (2014).

Variations in the time between tamoxifen treatment and behavior testing, or the age at tamoxifen treatment, could have influenced the consequences of disrupting oligodendroglia dynamics. However, no statistically significant relationships between these experimental time metrics and behavioral performance of P-Myrf^{-/-} was detected in our sample (Figure S2).

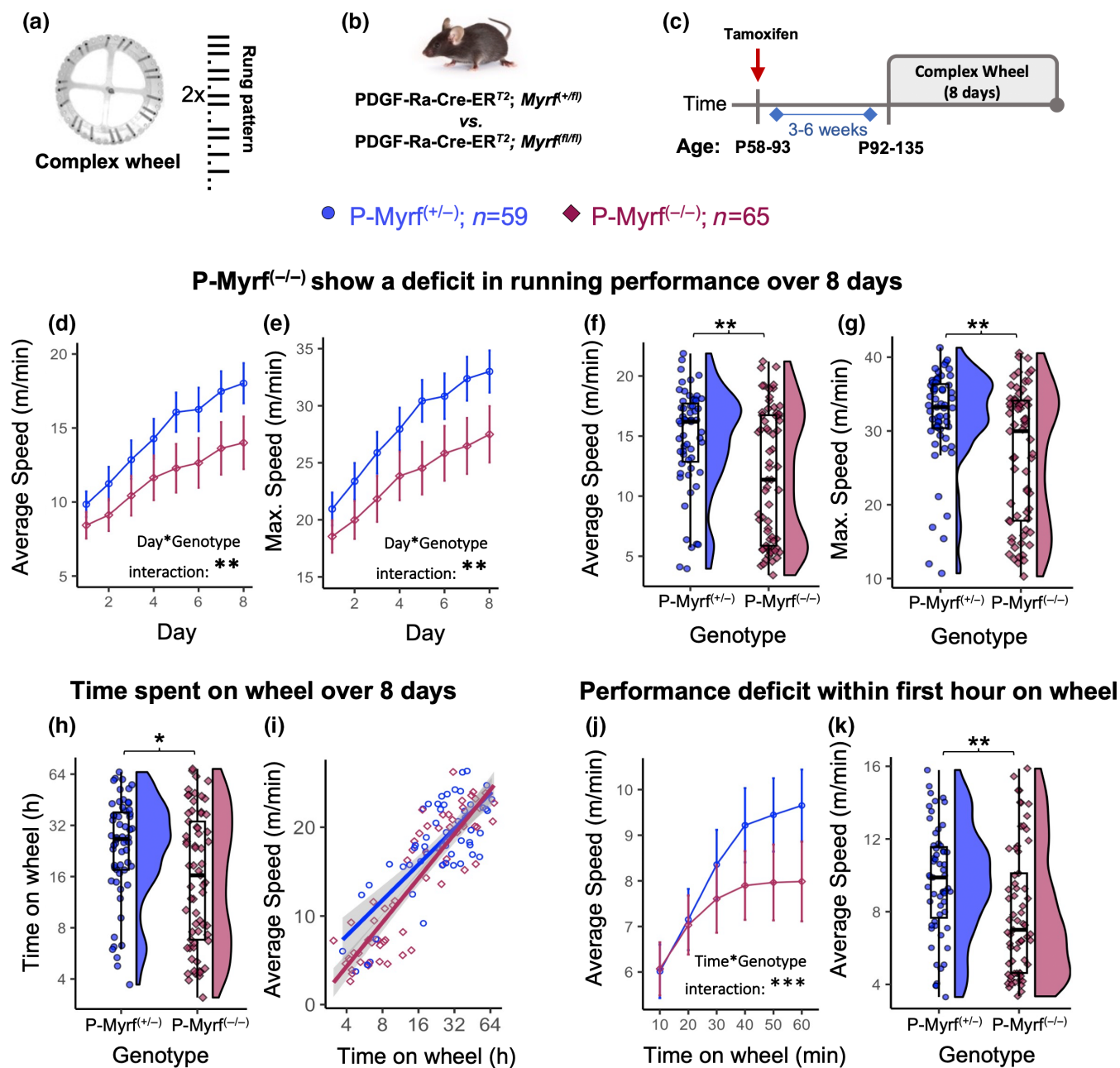


FIGURE 2 Impairment of performance on the complex wheel (CW) due to prevention of oligodendrocyte lineage differentiation. (a) Complex running wheel, with an irregular rung pattern displayed beside the wheel. (b) Animals bred on a PDGF-Rα-Cre-ER^{T2} with two floxed alleles of *Myrf* were compared with control animals that only have a single allele floxed. (c) Schematic illustration of experimental design. Animals were given free access to the CW for at least 8 days. (d, e) Comparing performance across chronological timeframe. (D) Mean average speed and (e) maximum speed on the CW of P-*Myrf*^(-/-) animals was statistically significantly lower across 8 days (mixed-ANOVA), indicated by a main effect of genotype and a genotype × day interaction across both speed metrics. (f, g) Raincloud plots of average (f) and maximum (g) speed across the 8 days of running showing a statistically significantly reduced performance in the P-*Myrf*^(-/-) sample. (h) P-*Myrf*^(-/-) spent statistically significantly less time running on the CW than their P-*Myrf*^(+/-) siblings over 8 days of testing. (i) Statistically significant log relationship between the average speed of animals on day 8 of testing and the time animals spent on the wheel during the 8 days (rho = .871 p < .001, Spearman's). (j) Average running speed plotted for the first hour (10 min intervals) that animals spent on the wheel. A statistically significant interaction of time and genotype indicated a lower performance of P-*Myrf*^(-/-) animals over early running attempts. (k) Average speed within 10 mins time period of wheel running after the first hour on the wheel. Data presented as Mean ± 95%CI or boxplots. Mixed-ANOVA (main factors: genotype, sex; factor: time) used for statistical comparison of performance over time comparison. Mann-Whitney *U* test used for statistical comparison of two groups. Asterisk indicate statistical significance (*p < .05, **p < .01, ***p < .001).

2.3 | P-Myrf^{-/-} animals spend less time running on the CW

As running on the wheel was voluntary and animals were given unrestricted access to the wheels, the time individual animals spent on the running wheel varied significantly. Time running on the wheel ranged from approximately 4 h to approximately 64 h in 8 days (Figure 2h). Overall, P-Myrf^{-/-} animals spent significantly less time running on the complex running wheel than P-Myrf^{+/-} (Mann-Whitney U: $p = .014$, Figure 2h, also see Figure S3a,b). Similar to other performance metrics across 8 days (Figure 2f,g), the time animals spent on the wheel had a wider and bimodal distribution in the P-Myrf^{-/-} group (Figure 2h).

Importantly, we found a statistically significant log-positive relationship between the time animals spent running on the wheel and their average running speed on day 8 of testing (Figure 2i, Spearman's rank correlation; across genotype, $\rho = .800$, $p < .001$; P-Myrf^{+/-}, $\rho = .627$, $p < .001$; P-Myrf^{-/-}, $\rho = .871$, $p < .001$). This strong relationship between task engagement and performance suggests that when considering running speed metrics over chronological time periods (e.g., days, Figure 2d-g) it might be important to account for variation in the time animals spent running on the wheel, and therefore inter-individual variation in the time available for learning the task.

2.4 | Deficit on complex running wheel detected within the first hours of running

Xiao et al. (2016) reported a deficit in the performance of P-Myrf^{-/-} animals on CW within the first 4 h of testing. However, in our study the time animals spent rotating the wheel within the first 4 h of testing ranged from about 5 min to over 2 h (Figure S3a). One way to account for such variation in task engagement is to compare running performance of animals against the time they spent on the wheel, rather than chronological time. Hence, we analyzed average running speed on the CW for the first hour animals spent rotating the wheel, regardless of when that running happened (Figure 2j,k). Using a mixed two-way ANOVA (main factors: genotype, sex; within subject factor: time (10 min intervals)), we found a significant effect of time ($F(2.21, 265.3) = 88.0$, $p < .001$) and a significant time \times genotype interaction for average daily speed ($F(2.21, 265.3) = 9.06$, $p < .001$, Figure 2j), indicating that P-Myrf^{-/-} animals showed less improvement in performance with practice over the first hour of running. The average running speed achieved in a 10 min interval after 1 h on the wheel was significantly lower in P-Myrf^{-/-} animals (Figure 2k, Mann-Whitney U: $p = .004$). Further analysis of animals' performance over the time they spent rotating the wheel are outlined in Figure S3c-f, comparing running speeds for longer timeframes.

Overall, these results replicate the main behavioral results obtained by McKenzie et al. (2014) and Xiao et al. (2016), indicating an early deficit in learning on the CW in animals with ablation of Myrf in OPCs during adulthood. However, unlike McKenzie et al. (2014),

we found wide variation in the amount of time animals spent engaging with the task, a factor that is important to take into account when interpreting behavioral changes. Taking this variation into account by considering time spent on wheel rather than chronological time, we found that ablation of oligodendrogenesis results in deficits in performance improvement over the first hour of experience on the wheel.

2.5 | Probing task demands of the CW task

To better understand the task demands of the wheel running task, we tested wild type (WT) mice on different variants of the wheel. Switching to a CW after running on the normal wheel leads to a partial reduction in running speed in WT mice (Figure S4), that recovers after a day or two of further training, indicating the task demand specific to the CW is mainly probed in the first couple of days of exposure to the wheel.

To test whether mice learn a specific sequence of movements to master the CW, we tested the effects of changing the rung sequence after exposure to one variant of the CW. This does not lead to reduction in running speed in WT mice (Figure S4), suggesting that mice learn a general strategy for running on irregularly spaced rungs, rather than a specific sequence of movements.

Taken together, these behavioral findings in WT mice suggest that learning to run at speed on a CW primarily involves adaptation to the irregular spaced rung positions, particularly during early task engagement.

2.6 | Ablation of oligodendrogenesis alters brain microstructure independently of wheel running

Previous work has reported alterations in WM microstructure, measured with magnetic resonance imaging (MRI) techniques, in response to motor learning (Sampaio-Baptista et al., 2013; Sampaio-Baptista et al., 2020). However, the underlying mechanism is unclear, as these changes could relate to remodeling of pre-existing myelin and/or recruitment of new OLs. Furthermore, the contribution of new OLs to MRI metrics has not been directly tested.

In the current study, we hypothesized that disruption of oligodendrogenesis in early adulthood affects brain microstructure, as it interferes with ongoing cellular dynamics and de novo myelination. Further, we hypothesized that learning to run on the CW affects brain microstructure. Finally, given evidence that adaptive oligodendrogenesis contributes to learning to run on the CW, we hypothesized that effects of CW running on brain microstructure should differ between knock-outs and controls.

We employed ex vivo MRI (see Methods) to compare P-Myrf^{-/-} ($n = 26$) and P-Myrf^{+/-} ($n = 25$) animals that had free access for 12 days to either the CW ($n = 26$) or to a fixed immovable CW in which running was not possible (from here on referred to as "fixed wheel", FW, $n = 25$; Figure 3a). This FW control condition was used to keep all environmental factors, other than wheel running, similar

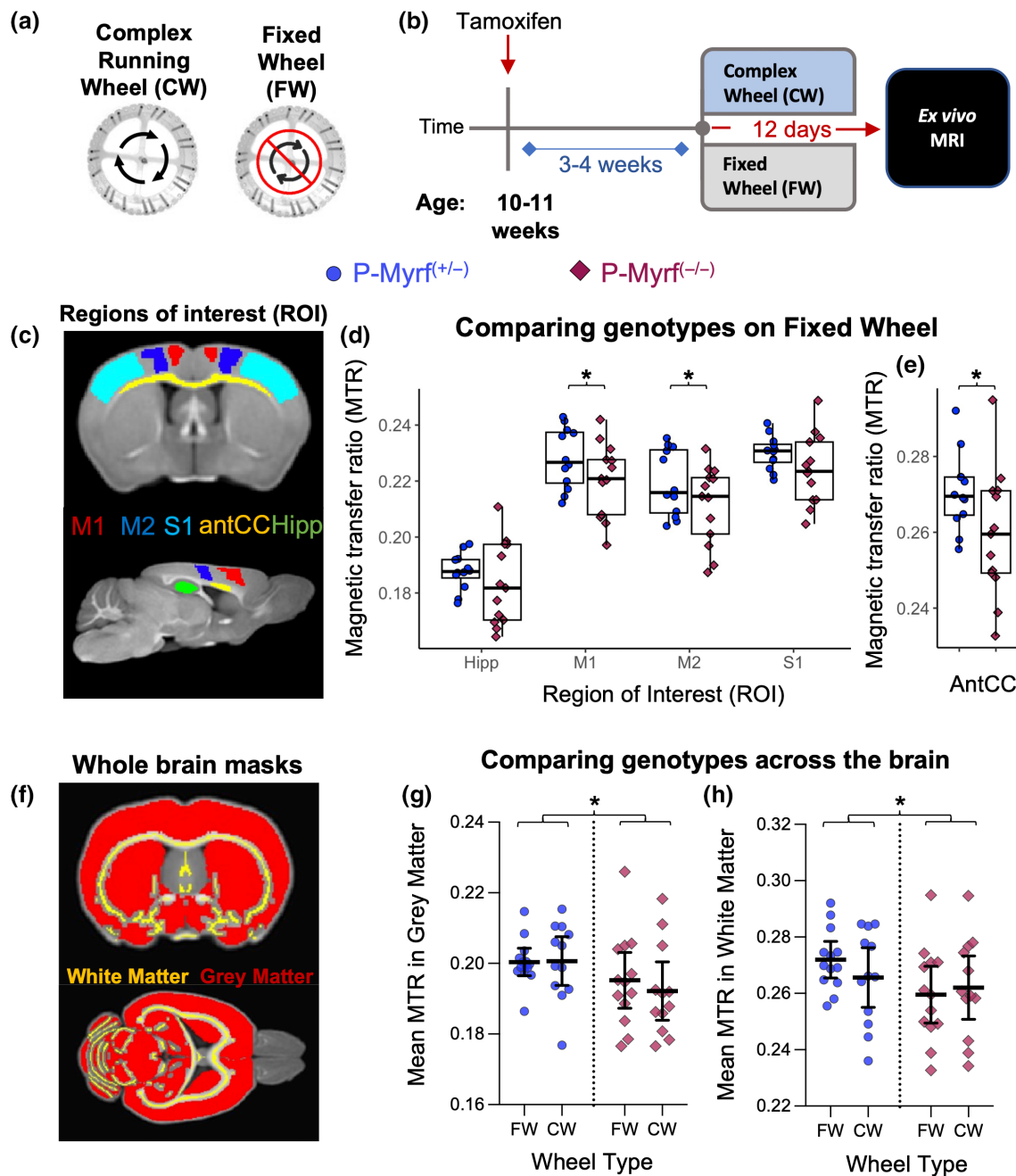


FIGURE 3 Ablation of oligodendrogenesis alters brain microstructure even in the absence of wheel running. (a) Illustration of experimental design. (b) Animals used for ex vivo MRI imaging were exposed to either a complex wheel (CW) on which they can run, or an immovable CW (fixed wheel, FW). (c) Coronal and sagittal section of magnetisation transfer ratio (MTR) image illustrating regions of interest (ROI) masks used for the ROI analysis. (d, e) For animals only exposed to the FW ($P-Myrf^{+/-}$, $n = 12$; $P-Myrf^{-/-}$, $n = 13$), ROI-specific mean MTR revealed that the ablation of oligodendrogenesis in the absence of wheel running lead to statistically significant changes in brain microstructure in the primary motor cortex (M1), secondary motor cortex (M2), and the (e) anterior corpus callosum (antCC). (f) Mask for the gray matter (GM, red) and white matter skeleton (WM, yellow) used for analysis. (g, h) MTR was reduced in (g) GM and the (h) WM skeleton for $P-Myrf^{-/-}$ animals compared with control animals, regardless of wheel condition ($P-Myrf^{+/-}$, $n = 25$; $P-Myrf^{-/-}$, $n = 25$). Diffusion-weighted parameters, such as FA and MD, did not reveal any statistically significant differences. See supporting information Figure S6 for more details. Data presented as mean \pm 95%CI or boxplots. Asterisk indicate statistical significance (* $p < .05$).

between groups (schematic illustration of experimental design, Figure 3b).

Brain microstructure was assessed ex vivo using a 9.4 T horizontal bore MR scanner (Varian, Palo Alto, CA, USA). Magnetisation transfer

imaging and diffusion-weighted imaging (DWI) were acquired. Three parameters were extracted (see Figure S5): (i) magnetisation transfer ratio (MTR), which allows indirect detection of water bound to macromolecules, such as lipids and proteins, and is thus sensitive to myelin

(Deloire-Grassin et al., 2000); (ii) fractional anisotropy (FA), which describes the anisotropy of diffusion of water molecules; and (iii) mean diffusivity (MD), which describes the rotationally invariant magnitude of water diffusion within brain tissue. FA and MD are sensitive but not specific to a number of WM features, such as myelin, axon caliber, density and organization, among others (Lazari & Lipp, 2021; Sampaio-Baptista & Johansen-Berg, 2017; Zatorre et al., 2012).

For a region of interest (ROI) analysis, five brain areas hypothesized to be involved in learning a running wheel task, or sensitive to exercise on the wheel, were selected: primary (M1) and secondary (M2) motor cortex, primary sensory cortex (S1), hippocampus (Hipp) and an anterior region of the corpus callosum (antCC), as illustrated in Figure 3c. For exploratory purposes, we ran voxel-wise analyses to test for more local effects in any brain area across the gray matter (GM) mask and WM skeleton (Figure 3f). Finally, to investigate global changes, we tested for effects averaged across the whole GM and whole WM skeleton (Figure 3g,h).

2.6.1 | Effects of genotype

First, to investigate the effect of the genetic manipulation on brain microstructure without considering behavioral experience of wheel running, we tested for effects of genotype in animals that were only exposed to the FW (our control condition, $n = 25$). When testing across the four GM ROIs (M1, M2, S1, Hipp), P-Myrf^{-/-} ($n = 13$) were found to have significantly lower MTR, compared with P-Myrf^{+/+} ($n = 12$) (mixed ANOVA; main effect of genotype ($F(1, 17) = 7.32$, $p = .015$)). Post-hoc tests for individual ROIs (ANOVA, Bonferroni adjusted for number of ROIs) found a significant reduction in MTR in M1 (Figure 3d, $p = .02$) and M2 (Figure 3d, $p = .032$). Additionally, for the WM region of the antCC, P-Myrf^{-/-} had significantly lower MTR, compared with P-Myrf^{+/+} (Figure 3e, $p = .013$). No statistically significant changes between groups were observed for diffusion-derived metrics of MD and FA (Figure 3b). No effects were found in the voxel-wise analysis.

2.6.2 | Effects of wheel condition

Next, to investigate the effect that running the CW for 12 days may have on brain microstructure, we tested for effects of wheel condition (fixed vs. CW) in P-Myrf^{+/+} control animals only (CW: $n = 13$, FW: $n = 12$). No statistically significant difference between the two running wheel groups were detected in MTR, FA or MD in the ROI analysis (Figure 3b). A voxel-wise analysis revealed an increase in MD in the left M1 GM region (Figure 3a,b) for P-Myrf^{+/+} that ran the CW.

2.6.3 | Interactions between genotype and wheel condition

Finally, to investigate potential interactions between genetic manipulation and behavioral experience, we performed an ANOVA with

genotype and wheel (CW and FW) as factors on all samples. Similar to effects found when considering the FW groups alone, significant main effects of genotype on MTR were found within specific GM and WM ROIs (M1, M2, S1, antCC; Figure 3a-e), as well as across the whole GM mask (Figure 3g; $F(1, 34) = 7.77$, $p = .019$) and the WM skeleton (Figure 3h; $F(1, 34) = 4.73$, $p = .037$), with P-Myrf^{-/-} animals having significantly lower MTR. However, no main effect of wheel or interactions between genotype and wheel on MTR were found. Further, no main effects or interactions were detected in FA or MD in the ROI analysis (Figure 3f-n). The voxel-wise analysis detected small clusters of changes in MTR between genotypes in cortical and midbrain regions (Figure 3c), yet no interaction between genotype and wheel was found for any voxel-wise analyses.

2.6.4 | Correlations between MRI and behavioral performance

A voxel-wise analysis across all animals in the CW condition ($n = 26$) tested for correlations between brain metrics and performance metrics (maximum speed and total distance run over 8 days). No relationship was found for MTR or FA. However, we found a negative correlation between distance run and MD in broad areas in cortical GM and basal ganglia, independent of genotype (Figure 3d,e). Mice that ran longer distances had lower MD, indicating that water in these areas is more restricted (regardless of direction), potentially indicating higher brain tissue density.

Taken together, these results indicate that the ablation of oligodendrogenesis in young adult mice for 5–6 weeks led to decreases in the myelin-sensitive metric MTR, across GM and WM regions. However, we found no interactions between wheel running and genotype, suggesting no evidence for changes in brain microstructure in response to wheel running that depends on oligodendrogenesis.

2.7 | Ablation of oligodendrogenesis changes oscillatory brain activity in Myrf-cKO mice in vivo

Previous work has indicated that even subtle deficits in myelination can lead to altered neuronal activity and synchronicity (Dubey et al., 2022; Gould et al., 2018; Kato et al., 2020), whereas modeling approaches indicate a role of activity-dependent myelination in oscillatory self-organization and homeostatic coordination of brain networks (Noori et al., 2020; Talidou et al., 2022).

As our histological and MRI data suggests alterations related to myelination in P-Myrf^{-/-} mice, we tested oscillatory brain activity using cortical electroencephalogram (EEG) recordings in freely behaving P-Myrf mice, not exposed to running wheels. In each animal, the electrodes were implanted in two cortical regions (see Figure 4a) at the age of P110–120, 5–6 weeks after tamoxifen treatment (Figure 4b). Mice were individually housed in standard conditions. Data were recorded over a 2-day period, 1–2 weeks after surgery (P-Myrf^{+/+}: $n = 3$, P-Myrf^{-/-}: $n = 4$) during spontaneous sleep and waking in undisturbed animals.

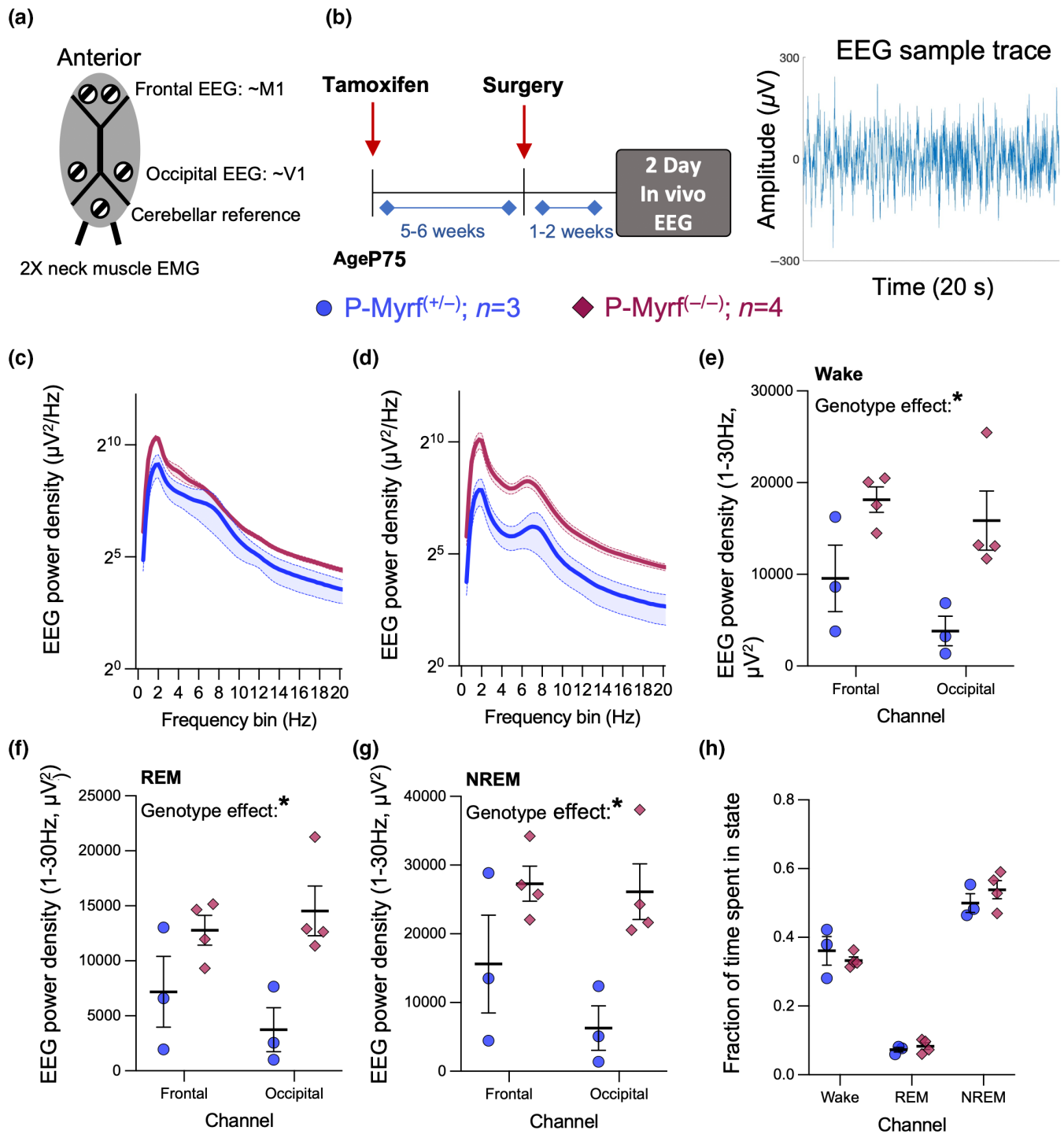


FIGURE 4 Ablation of oligodendrogenesis alters brain activity in the absence wheel running. (a) Schematic illustration of the location of screws implanted for in vivo electroencephalogram (EEG) recording. (b) Schematic illustration of experimental design. (c, d) Mean group EEG power density by Frequency during wakefulness in (c) frontal channel and (d) occipital channels. Data presented as Mean \pm SED (e) EEG power density in the 1–30 Hz frequency band was higher for animals with ablated oligodendrogenesis in the frontal and occipital channels during wakefulness. This genotype difference was found to be statistically significant across frontal and occipital channels (mixed ANOVA) during wakefulness. (f, g) The effect was not specific to wakefulness, as statistically significant differences in EEG power density were also observed during (f) REM sleep and (g) non-REM sleep. (h) The fraction of time animals spend in different vigilance states. Recordings were undertaken in seven male adult mice (*P-Myrf*^(-/-); *n* = 4; *P-Myrf*^(+/-); *n* = 3). Data presented as Mean \pm SEM. Asterix indicate statistical significance (**p* < .05).

Spectral analysis revealed a significant increase in EEG spectral power across broad frequency bands in *P-Myrf*^(-/-) animals in the frontal and occipital region during wakefulness (Figure 4c–e), when

compared with *P-Myrf*^(+/-) animals. Using a mixed ANOVA (main effect: genotype, within-subject factor: electrode location), the genotype difference in total EEG power density in 1–30 Hz frequency range

was statistically significant across both cortical derivations during wakefulness (main effect for genotype: $F(1, 5) = 10.4, p = .023$). This change in total spectral power induced by the conditional deletion of *Myrf* in OPCs was also observed during other vigilance states such as REM sleep (Figures 4f and S8a,b; $F(1, 5) = 12.7, p = .016$) and nonREM sleep (Figures 4g and S8c,d; $F(1, 5) = 11.4, p = .02$). The fraction of time animals spent in different vigilance states did not differ between genotypes (Figure 4h). The peak EEG power density during wake and REM sleep (0.25 Hz resolution) in the theta range (4–12 Hz) was significantly different between genotype groups ($F(1, 5) = 7.4, p = .041$, Figure S8e), yet the frequency of the peak was not (Figure S8f). Altogether, these results provide evidence for changes in brain electrophysiology induced by the ablation of oligodendrogenesis for 7–8 weeks prior to EEG recording in freely moving and behaviorally naive mice.

In summary, we replicated the previously reported behavioral phenotype of P-*Myrf*^{f/f-/-} showing reduced capacity to improve performance over time on the CW, which is prominent within the first hour of running on the wheel. We additionally found a high degree of variation in engagement with the wheel, which should be taken into account when interpreting results. Further, our results suggest that ablation of oligodendrogenesis alters brain microstructure, as detected by a reduction in MTR, and brain activity, as indicated by increase in EEG mean spectral power, independently of behavioral experience on the complex running wheel. This suggests ablation of oligodendrogenesis in P-*Myrf*^{f/f-/-} can itself lead to physiological and structural alterations in the brain.

3 | DISCUSSION

This study investigated the consequences of disrupting OL differentiation during adulthood (Figure 1) on behavior (Figure 2), brain structure (Figure 3), and brain activity (Figure 4). Our results replicated the key finding that ability to perform a CW running task is disrupted by ablation of oligodendrogenesis (McKenzie et al., 2014; Xiao et al., 2016) (Figure 2). These group differences on the CW were present within the first hour of running on the wheel. Additionally, using an ex vivo MRI (Figure 3) and in vivo EEG (Figure 4), we found that the ablation of oligodendrogenesis altered brain microstructure and activity independently of the behavioral experience of running the CW. Taken together, our findings indicate that inhibiting the formation of new OLs in adult mice not only led to a decline in performance on the CW but also brought about alterations in both the microstructure and activity of the brain, irrespective of animals' experience with the task. Whether and how these task-independent changes in brain microstructure and function contributed to the observed behavioral phenotype requires further investigation.

3.1 | Replication of behavioral deficit on the CW

Our results replicate findings indicating a performance deficit of P-*Myrf*^{f/f-/-} on the complex running wheel over 8 days (McKenzie

et al., 2014). However, we found large variability in the time animals spent engaging with the CW task (Figure 2h), which was in turn related to their overall performance (Figure 2i). This highlights the difficulty of separating wheel engagement from skill learning when interpreting task performance in this voluntary task. Accounting for this variability by analyzing performance on the CW as a function of time animals spent on the CW (Figures 2j,k and S3c–f) revealed that P-*Myrf*^{f/f-/-} animal's deficit on the wheel arises within the first hour of engagement with the task (Figure 2j), a result replicating previous findings indicating an early deficit (Xiao et al., 2016).

However, it is difficult to clearly define the underlying deficit in P-*Myrf*^{f/f-/-} mice that leads to the observed deficit on the CW, as the task demands of the CW are multifaceted. Running speed improvements over several days are observed on both the normal and CW and can therefore reflect generic aspects of wheel exposure as well as specific demands of the CW (Figures S1d and S4). Switching from a normal wheel to a CW leads to a temporary reduction in running performance in WT mice (Figure S4a, Hibbits et al., 2009), indicating there is some specific task demand of the irregular spaced rungs in the initial task engagement. Yet, changing the rung sequence does not affect performance, indicating that mice adapt a strategy to cope with irregular spaced rungs in general and do not learn a specific sequence (Figure S4). Together, this indicates that mice need to find a new strategy (e.g., adapt their gait pattern, McKenzie et al., 2014) to cope with irregular rungs and be able to run and improve their performance on the CW.

A deficit within the first hour running the CW suggests that a key task requirement impaired in P-*Myrf*^{f/f-/-} animals is probed by early attempts to perform the CW task, rather than by learning processes evolving over several hours or days. Although the CW has been used as a test of subtle deficits in complex motor execution (Hibbits et al., 2009; Liebetanz et al., 2007; Schalomom & Wahlsten, 2002), the fact that P-*Myrf*^{f/f-/-} mice already trained on the CW prior to tamoxifen treatment have no deficits when re-exposed to the CW (McKenzie et al., 2014), together with the absence of any execution deficit on other motor tasks (Figure S1a–f, McKenzie et al., 2014), suggests that impairment that we and others have found in CW performance reflects impairment in the acquisition of a new skill rather than skill execution or general motor performance.

3.2 | Task-independent changes to brain structure and function might contribute to behavioral deficit

How an inability to form new OLs can cause the observed learning phenotype of P-*Myrf*^{f/f-/-} mice within just a few hours is unclear. Previous studies suggest that rapid production of *Enpp6*-expressing immature OLs can be observed within the first hours of exposure to the CW, potentially contributing to circuit functioning and neuronal metabolism (Xiao et al., 2016). Yet, our understanding of how new OLs contribute to skill learning and memory formation remains incomplete, with apparently different timescales of involvement found with different learning paradigms. For example, while early learning deficits



have been found with CW running, studies investigating spatial learning and fear conditioning in mice with a conditional knockout of *Myrf* in OPCs found no deficit in early memory formation, but a deficit of memory consolidation over days or weeks (Pan et al., 2020; Shimizu et al., 2023; Steadman et al., 2020). Additionally, different aspects of myelin plasticity might occur over distinct timescales. For example, a study investigating motor learning in the dextrous reaching task found modulation of existing myelin in upper layers of M1 predominant in early stages of learning, whereas addition of new myelin sheaths was more relevant post learning (Bacmeister et al., 2022).

An alternative explanation for the behavioral deficit is that the disruption of oligodendrogenesis for weeks prior to behavior testing in P-*Myrf*^{-/-} caused subtle changes in brain microstructure (Figure 3) and activity (Figure 4) which then impacted on capacity to learn a new skill. New OLs continue to differentiate throughout early adulthood (Hill et al., 2018; Hughes et al., 2018; Rivers et al., 2008; Young et al., 2013) and interfering with such ongoing cellular dynamics can have unintended consequences, as suggested by the current study (Figures 3 and 4). Activity-regulated myelination, including oligodendrogenesis, is proposed to play a role in homeostatic coordination and oscillatory self-organization in local and large-scale brain networks (Dubey et al., 2022; Noori et al., 2020; Talidou et al., 2022) and mild impairments in myelination have been linked to decreased motor learning by increasing asynchrony and spontaneity in neural activity (Kato et al., 2020). Hence, it is possible that brain differences between genotype groups at the start of behavioral testing, as well as a lack of activity-dependent up-regulation of oligodendrogenesis triggered by exposure to the CW, might have combined to contribute to the observed behavioral phenotype.

3.3 | Changes in brain microstructure due to *Myrf* knock-out

When investigating the consequences of genetic ablation of OL differentiation on brain microstructure using an ex vivo MRI, we found significantly lower MTR in multiple brain regions (Figure 3). We hypothesized that disruption of oligodendrogenesis will affect brain microstructure, as it disrupts ongoing cellular dynamics and myelin formation. As MTR is related to myelin content of tissue (Lazari & Lipp, 2021), lower MTR may reflect reduction in myelination caused by the significant reduction in new oligodendrocyte formation (Figure 1) induced for ~5–6 weeks prior to ex vivo MRI. However, estimating how much myelin content was added during the timeframe of interest is difficult and requires further histological investigation. Further, it is not clear if the disruption of oligodendrocyte formation can lead to relevant inflammatory responses that might have influenced MRI and even behavioral results, which is a limitation of this study. However, MRI metrics derived from DWI (FA, MD), that are sensitive to tissue microstructure and less sensitive or specific to myelin, were not significantly affected by the deletion of *Myrf* (Figure S6). The finding that changes in MTR were widespread across WM and

GM regions is consistent with the global ablation of OL differentiation across the whole CNS.

We found no evidence for task-dependent changes in brain microstructure related to myelination when investigating how motor learning on the CW affected brain microstructure (in comparison to a FW control condition). Specifically, we found no effect of CW running on the myelin-sensitive metric MTR (Figure 3, Figure S6), regardless of whether animals had disrupted oligodendrogenesis. We had hypothesized that motor learning should lead to changes in myelin-sensitive metrics of brain microstructure if associated with increase in myelination, as previously reported in the context of the skilled reaching motor learning tasks in rats (Sampaio-Baptista et al., 2013). However, there are several important methodological differences between these studies, including species (rat vs. mouse) and training task. The reaching task involves the development of fine motor movements in comparison with the gross motor movements necessary to perform the CW task. Furthermore, MRI techniques employed here can only measure cellular effects very indirectly and are less sensitive to small effects compared with histological approaches employed by others, which showed increased OLs differentiation in motor cortex and subcortical WM due to CW running (McKenzie et al., 2014; Xiao et al., 2016). In addition, the fixed wheel control condition we employed might have offered more environmental enrichment in comparison with home cage controls that are typically used (Keiner et al., 2017).

Furthermore, it is possible that at the time point of our measurement, immediately after 12 days of training on the CW, experience-induced changes in myelination might not have been prominent enough to cause detectable changes in MTR. Taken together, we did not find evidence for learning-induced changes in myelin sensitive MRI measures of brain microstructure after learning to run the CW.

3.4 | Electrophysiological changes cause by *Myrf* knockout

In addition to genotype differences in microstructure, deletion of *Myrf* in OPCs caused alterations in oscillatory brain activity (Figure 4), as reflected in higher EEG power density across broad frequency bands. Increases in spectral power of LFPs have been reported in Plp1-KO models with mild myelin deficits (Gould et al., 2018) and cuprizone models of demyelination (Dubey et al., 2022). Associated computational modeling indicated that a decrease in conduction velocity, as a result of reduced myelination, can lead to an increase in spectral power (Gould et al., 2018). Additionally, adaptive myelination, disrupted in P-*Myrf*^{-/-} animals, might regulate homeostatic coordination and oscillatory self-organization in local and large-scale brain networks (Dubey et al., 2022; Noori et al., 2020; Talidou et al., 2022). Hence, it is plausible that reduced myelination and disruption of adaptive myelination, caused by ablated oligodendrogenesis over a 6–7 week period, led to the observed increases in EEG power density. However, identification of the underlying mechanism driving such broad alterations in brain activity requires further investigation.

3.5 | Summary and conclusion

In summary, the findings presented in this study suggest that ablation of oligodendrogenesis by conditional deletion of *Myrf* in PDGFA-positive OPCs leads to subtle but detectable physiological and structural differences in the brain. The previously detected, and here replicated, behavioral deficit on the complex running wheel might therefore partly arise as a result of these task-independent brain differences, in addition to impairments in oligodendrogenesis driven by learning.

The current findings raise many questions for future work. For example, the timescale over which these structural and physiological changes develop should be explored as we only sampled effects at a single time point. Further, it remains to be tested whether the effects found here hold for other transgenic models of disrupted oligodendrogenesis. Although the use of such models has thus far been predominantly to study of effects on learning, future work could investigate whether and how continuous oligodendrogenesis plays a broader role in maintaining brain microstructure and function. Overall, this study suggests that the implications of disrupting oligodendrogenesis in the adult mouse brain extend beyond specific task-related effects and should be taken into account when interpreting behavioral phenotypes and designing future experiments.

4 | MATERIALS AND METHODS

4.1 | Animals

All work carried out conformed to UK Home Office legislation (Scientific Procedures Act 1986).

4.1.1 | Mouse breeding and genetic background

Mice used in this study were originally generated in the Richardson laboratory (McKenzie et al., 2014), UCL by crossing *Pdgfra-CreER^{T2}* transgenic mice (Rivers et al., 2008) with Cre-conditional reporter mice *Rosa26R-YFP* (*R26R-YFP*) (Srinivas et al., 2001) to generate double-homozygous offspring. Cre and YFP reporter lines in the Richardson Laboratory were maintained separately by crossing (more than 10 generations) with C57B6 females (Charles River; Margate, UK). These *Pdgfra-CreER^{T2}*; *Rosa26R-YFP* were crossed with *Myrf^(fl/fl)* mice (Emery et al., 2009) to obtain *Pdgfra-CreER^{T2}*; *R26R: Myrf^(+/fl)* offspring, which were sibling-mated to obtain *Myrf^(fl/fl)* and *Myrf^(+/fl)* littermates. These animals were finally crossed to generate cohorts of *Pdgfra-CreER^{T2}*; *R26R-YFP: Myrf^(fl/fl)* and *Myrf^(+/fl)* littermates for behavioral testing and further breeding. In the Richardson Laboratory, *Myrf^(fl/fl)* mice were obtained originally (in 2010) on a mixed 129/CBA/C57B6 background.

Five breeding pairs of *Pdgfra-CreER^{T2}*; *R26R-YFP: Myrf^(fl/fl)* and *Pdgfra-CreER^{T2}*; *R26R-YFP: Myrf^(+/fl)* (referred to as P-*Myrf^(fl/fl)* and P-*Myrf^(+/fl)*) were sent to our laboratory from the Richardson Lab, UCL in 2016 and were used to breed animals for our study by crossing

P-*Myrf^(fl/fl)* with P-*Myrf^(+/fl)* mates. Mice carried copies of *Pdgfra-CreER^{T2}* on both alleles and were either *R26R-YFP^(+/-)* or *R26R-YFP^(+/+)*. Two generations of animals were bred before behavior testing started for the current studies and animals from a total of four consecutive generations were used for behavior testing. Hence, P-*Myrf^(fl/fl)* and P-*Myrf^(+/fl)* were maintained by sibling crossing for six generations in our facilities.

For testing the normal and CW running in WT mice, 20 C57BL/6JOLA-Hsd mice (8 males and 8 females) were purchased from Envigo, UK at age P60. The mice were given a 1-week period to acclimate before commencing behavioral testing.

4.1.2 | Mouse genotyping

Genotyping for Cre-ER^{T2} (Cre 5'-TCG ATG CAA CGA GTG ATG AG and Cre 3'-TTC GGC TAT ACG TAA CAG GG; Product Size 481 bp) and *R26R-YFP* (*R26WTF1-AAA* GTC GCT CTG AGT TGT TAT, *R26WTR1-GGA* GCG GGA GAA ATG GAT ATG, *R26KOF1-GCG* AAG AGT TTG TCC TCA ACC) was done by PCR amplification of genomic DNA. *Myrf^(fl/fl)* mice were genotyped by PCR amplification of genomic DNA using primers within intron 7 flanking the first lox site (5'-AGGAGTGTGTGGGAA-GTGG and 5'-CCCAGGCTGAA-GATGGAATA), which gives a 281 bp product for the WT allele and a 489 bp product for the loxP-flanked allele (Emery et al., 2009).

4.1.3 | Tamoxifen administration

Tamoxifen (Sigma T5648) was dissolved at 40 mg/mL in corn oil on a shaker overnight at RT and by subsequent sonicating at 21°C for 1 h. P-*Myrf^(+/-)* and P-*Myrf^(-/-)* mice were generated by administering tamoxifen (0.3 mg/g body weight in corn oil) by oral gavage for 4 consecutive days to *Pdgfra-CreER^{T2}*; *R26R-YFP: Myrf^(floX/floX)* and *Pdgfra-CreER^{T2}*; *R26R-YFP: Myrf^(+/floX)*. Animals were left for at least 2 weeks before experimental procedures. During, and for a week after tamoxifen treatment, nutritious jelly and mash were provided for all mice to prevent excessive weight loss because of the adverse effects of the drug.

4.2 | Behavior testing of mice

Assessment of behavioral phenotype was conducted by the same researcher. Wherever possible, equal numbers of animals of each sex were included in each experimental group. Researchers were blinded to the genotype of the animals during data analysis and collection. All mice were maintained on a 12 h artificial light-dark cycle (9:00–21:00). Food and water were provided ad libitum.

4.2.1 | Complex running wheel

Cages with running wheels were purchased from Lafayette Neuroscience (Scurry mouse mis-step wheel Model 80821S). This voluntary



running wheel cage comes equipped with a wheel (circumference = 0.389 m) that allows individual rungs to be removed to create a CW or rung configuration (Liebetanz et al., 2007; McKenzie et al., 2014). The mice were provided with a “complex wheel” (CW) with 16 out of 38 rungs removed to create a wheel with an irregular pattern of 22 rungs (Figure 2a), a configuration that was adapted from McKenzie et al. (2014). For behavior testing, mice were single caged with the running wheel, a paper house filled with nesting material and wood shavings to cover the floor of the cage. Mice were accustomed to the cage for 0.5 to 2 h before being provided access to the running wheel at the around the start of the dark period (~8.30 pm) by removing a dividing wall to the compartment where the wheel was located. Mice ran spontaneously, without artificial reward. Food and water were available ad libitum within the specialized running wheel cages.

Infrared sensors recorded wheel rotation, which allowed computer-controlled recording of wheel rotation as a function of time for 20 cages simultaneously for 24 h a day (The Scurry Activity Monitoring Software, Lafayette Neuroscience, Model 86165). For data analysis, counts of full wheel rotations were exported into a spreadsheet, divided into time bins of 10 s. Custom R scripts were used to extract the following running parameters from the baseline activity data: (1) Distance traveled, which represents the total number of wheel rotations \times wheel circumference. (2) Active intervals, which represent the number of 10 s intervals in which at least one full wheel rotation was recorded. (3) Average speed, which represents the sum of the distance run divided by the number of active intervals. (4) Maximum speed, which was calculated by determining the average speed in the 1% of fastest intervals run. Analysis of performance was conducted for either chronological time intervals (length of time vector) or for intervals of time that animals spent running on the wheel (length of vector containing only active intervals on the wheel).

Running speed of animals (distance/time) was conducted using time bins of 10 s. McKenzie et al. (2014) calculated the average running speed by quantifying wheel spins during a 1 min time bin. Yet, in the current study between 35% and 40% of continuous running bouts were found to be shorter than 1 min long (data not shown). That meant that average running speed was often not accurately estimated when using 1 min intervals to calculate speed.

4.2.2 | Complex running wheel and FW testing for ex vivo MRI experiment

A total of 24 animals were tested on the complex running wheel (P-Myrf^{+/−}; $n = 12$, 5 females; P-Myrf^{−/−}; $n = 12$, 4 females) in specific running wheel cages as described above. Additionally, 25 littermates were exposed to a static fixed CW that was not able to rotate (referred to as FW) in cages with otherwise identical set up (P-Myrf^{+/−}; $n = 12$, 4 females; P-Myrf^{−/−}; $n = 13$, 5 females). As the FW had the same missing rungs pattern that allows animals to pass between rungs, animals could climb and interact with the wheel as a kind of environmental enrichment yet could not run and turn the wheel. The

experiment consisted of five distinct batches of P-Myrf animals bred from the same set of five breeding pairs over consecutive litters. Littermates were semi-randomly assigned to cages equipped with either a CW or a FW and were tested in the same environment and time-frame. Semi-random assignment meant that animals were randomly assigned to a wheel type, while attempting to balance the numbers of genotype, sex and littermates equally between experimental groups.

4.2.3 | Accelerating RotaRod

Mice were tested on a standard RotaRod apparatus (Ugo Basile, Italy) with a 3 cm diameter rod. The setup allowed for simultaneous testing of up to three mice. Mice were habituated to the testing environment for 30 min and underwent three trial runs on the RotaRod at a constant speed of 4 rpm 2 days before the actual testing. Each trial lasted 120 s. On test day, mice were held by the tail and positioned on the rotating rod. After 10 s of adjustment, the rod's speed was incrementally increased from 4 to 40 rpm over the course of the trial. The duration each mouse remained on the rod was timed from the start of acceleration until the mouse fell or until 150 s, whichever occurred first. Each mouse underwent three trials with a 10 min rest between trials. The time to fall was recorded for each trial, with a maximum recorded time of 150 s. Testing was conducted during a controlled light period, between 2 and 5 pm.

4.2.4 | Balance beam

The test was conducted using a round wooden beam, either 15 or 7.5 mm in diameter, elevated 50 cm above the floor with a soft pad. The beam was angled approximately 10° to encourage voluntary crossing from the home cage to the testing area. Mice were acclimatized to the testing environment for 1 h by placing their cage within the testing room, which was dimly lit with a 60 W light. Training involved allowing mice to freely cross from their home cage to the opposite side of the beam. Each mouse underwent three trials with at least a 1 min rest between attempts. Training confirmed that mice learned to locate their home cage and cross without stopping or turning. Mice were tested first on the wider beam (1.5 cm diameter) and then on the narrower beam (0.75 cm diameter), with a 5 min rest in the home cage between tests. The test sequence was video recorded under dim lighting between 2 and 5 pm. Parameters such as the number of foot slips and steps taken to cross the beam were quantified. Each mouse was tested once, and the apparatus was cleaned with ethanol (70%) between tests.

4.3 | Perfusion of animals and tissue processing

Animals were deeply anesthetized (Euthatal: 80 mg/kg, i.p) with sodium pentobarbital and transcardially perfused with 10 mL PBS, followed by 30 mL paraformaldehyde (4% w/v in 0.1 M phosphate buffer) with the help of a perfusion pump (flow rate: 4 mL/min). After

perfusion, animal skulls were dissected by removing soft tissue from the outside of the skull (skin, muscle, eyes, etc.) and the lower jaws. Dissected skulls containing the CNS tissue were stored overnight in 4% PFA at 4°C for 24 h. Samples were then washed with phosphate buffer saline (PBS) before being stored in PBS at 4°C. Samples were sent to the Center for Image Sciences, UMCU, Utrecht, Netherlands for MRI. After MR imaging, tissue samples were sent back to the University of Oxford, cryoprotected with 30% sucrose solution, embedded in OCT and stored at -80°C until processed for histological analysis.

4.3.1 | Immunohistochemistry of free-floating brain sections

For Immunohistochemical analysis, coronal cryosections (30 µm) were cut (anterior to posterior) from the first section at which the antCC was visible and continuously connected from one hemisphere to the other. Brain sections were collected and washed in Tris-buffered saline (TBS; Sigma) and processed as floating sections. All incubations and washes were performed on a shaker at 60 rpm. Sections were blocked in TBS containing 10% normal goat serum (Sigma), 0.5% Triton-X (Sigma), and 1% BSA for 2 h at room temperature. The primary antibodies used were anti-PDGF-Ra (rabbit, New England Biolabs, 1:400 dilution), anti-APC (clone CC1; mouse, Calbiochem, 1:200 dilution), and/or anti-GFP (YFP) (chicken, Avas, 1:500), which were diluted in TBS containing 10% of the blocking solution (see above) at 4°C. Samples were then incubated with corresponding fluorophore conjugated secondary antibodies (1:500, Alexa FluorO-488 or 546, Thermo Fischer Scientific), diluted in blocking solution (1:10) for 2 h at room temperature. Samples were mounted and dried for ~10 mins before being sealed under a glass cover with Vectorshield anti-fade mounting medium (Vectorshield laboratories) and viewed by a Zeiss L subse SM-700 confocal microscope and ZEN software. Cells were counted in low-magnification photomicrographs (×20 objective) of nonoverlapping fields of coronal sections (320 mm × 320 mm each) of the corpus callosum, between the dorsolateral corners of the lateral ventricles (six fields per section, three sections per animal), as illustrated in Figure S9. The surface area of corpus callosum was calculated for each animal to determine cellular density. Image analysis was performed using Fuji/ImageJ (NIH).

4.4 | Statistical analysis of histological and behavioral data

4.4.1 | Criteria for excluding animals from CW data analysis

Previous experiments reveal that a small subset of healthy untreated animals show unusually low engagement in voluntary wheel running. To prevent such outliers from skewing overall group performance, we set the following pre-determined exclusion criteria for analysis of CW behavior performance: animals were excluded from the analysis

if: (1) they ran less than 1 km in 8 days ($P\text{-Myrf}^{+/+/-}$; $n = 4$, females; $P\text{-Myrf}^{+/-/-}$; $n = 1$), or (2) ran less than 100 m per day for at least half of the days recorded ($P\text{-Myrf}^{+/+/-}$; $n = 2$, females; $P\text{-Myrf}^{+/-/-}$; $n = 1$). In total, that led to the exclusion of eight animals based on these criteria ($P\text{-Myrf}^{+/+/-}$; $n = 6$; $P\text{-Myrf}^{+/-/-}$; $n = 2$).

4.4.2 | Testing for the effect of covariates on CW running

Before analyzing the impact of genotype on behavior, we assessed several covariates for their potential effects on CW running performance. First, to test for a potential effect of the generations and sex on the performance on the CW, a mixed two-way ANOVA (within subject factor: days (over 8 days of running); between subject factors: sex, generation) was used to analyze daily running speed (average or maximum). This analysis revealed that sex, but not generation, had a significant effect maximum running speeds (sex: $F(1, 116) = 22.68$, $p < .001$) on the CW, with females consistently outperforming males (Figure S1g). Apart from consistently running longer distances on the CW (total distance in meters: female, $M \pm SD = 35,505 \pm 22,374$; males, $M \pm SD = 16,413 \pm 14,426$), females also spent more time on the CW than males over a period of eight consecutive days (Figure S1h). While there was an expected difference in body weight between sexes, there was no difference in body weight between $P\text{-Myrf}^{+/-/-}$ and $P\text{-Myrf}^{+/+/-}$ animals for either sex at the start of behavior testing (body weight in grams: male- $\text{Myrf}^{+/+}$, $M \pm SD = 24.1 \pm 3.4$; male- $\text{Myrf}^{+/-/-}$, $M \pm SD = 24.3 \pm 2.4$; female- $\text{Myrf}^{+/+/-}$, $M \pm SD = 19.7.1 \pm 1.4$; female- $\text{Myrf}^{+/-/-}$, $M \pm SD = 19.4 \pm 2.3$).

The main analysis of behavioral performance on the CW combines data from several experiments. Hence, the age of tamoxifen treatment (range: P58–93, $M \pm SD = 77.11 \pm 8.6$), the age at behavior testing (range: P92–135, $M \pm SD = 109.9 \pm 7.9$) and the days between tamoxifen treatment and behavior testing (range: P21–43, $M \pm SD = 32.8 \pm 7.5$) varied between animals, experiments and generations (Table S1). However, we found no statistically significant correlation between the performance of the $P\text{-Myrf}^{+/-/-}$ on the CW (average running speed) and any of the age parameters mentioned above in the compiled data set of all $P\text{-Myrf}$ animals (Figure S2). Yet, it is of note that our experiments were not specifically designed to compare the effect of these age parameters on running performance.

In summary, of the potential covariates tested, only sex was found to be significantly associated with running behavior and so this factor was included as a fixed factor in all subsequent analyses of genotype differences to control for the induced variability.

4.4.3 | Statistical analysis method

Statistical analysis was performed using R (R Core Team, 2021), using the *rstatix* (0.7.2; Kassambara, 2023) and the *psycho* (v0.6.2; Makowski, 2021) packages. The statistical tests used for a particular analysis are mentioned during the data presentation in the result



sections. Normality of the data and assumptions of homogeneity of variance were tested (e.g., with Levene's test) before using parametric statistical analysis. If these assumptions were not met, nonparametric alternative tests were used for statistical analysis, or the test parameters were adjusted to account for the lack of homogeneity of variances (e.g., using unpooled variances and a correction to the degrees of freedom for unpaired *t*-test) whenever possible. If the assumption of sphericity (Mauchly's test) was violated in the mixed two-way ANOVA, Greenhouse–Geisser procedures were used to estimate epsilon in order to correct the degrees of freedom of the *F*-distribution. In this case, adjusted degrees of freedom are presented. Asterisks are used to indicate statistical significance when appropriate: * = $p < .05$, ** = $p < .01$, *** = $p < .001$. Details of statistical analysis approaches and results for each dataset are provided in Table S2.

4.5 | MRI methods

4.5.1 | MRI acquisition

Post-mortem high-resolution structural MRI was performed on a 9.4 T horizontal bore MR system (Varian, Palo Alto, CA, USA) at the Center for Image Sciences, UMCU, Utrecht, Netherlands, equipped with a 6 cm ID gradient insert with gradients up to 1 T/m. A custom-made solenoid coil with an internal diameter of 2.6 cm was used for excitation and reception of the MR signal. Three perfusion-fixed brains were inserted with the skulls intact in a custom-made holder and immersed in nonmagnetic oil (Fomblin, Solvay Solexis).

DWI was acquired with 3D eight shot spin-echo EPI sequence with the following parameters: 60 diffusion encoding directions; 1 average per image; 5 images with no diffusion weighting; TR/TE 500/38.6 ms, field of view: $24 \times 20 \times 20$ mm; isotropic resolution of 0.125 mm; d/Δ 5.5/8.91 ms, diffusion gradient strength (half-sine shape) 73 G/cm, $b = 3522$ s/mm²; total acquisition time 12.3 h.

Magnetization transfer images were also acquired with a 3D eight shot spin-echo EPI sequence with a train of saturating pulses in front of the image acquisition saturating frequencies 5, 10, and 100 kHz off resonance. Four volumes per frequency offset were acquired (TR/TE 500/28 ms; field of view: $24 \times 20 \times 20$ mm; resolution of 0.125 mm isotropic; total time 2.3 h).

A total of 71 animals were scanned for ex vivo MRI. Unfortunately, a subsets of 20 animals were perfused by a different experimenters using a different perfusion methods. Because of complications with the perfusion method and a significant deviation in measured MRI metrics from the remaining cohort, these 20 samples had to be excluded from the analysis.

4.5.2 | MRI data processing

All data were Fourier transformed and combined using the home-written software in MatLab (Mathworks®) from the Dijkhuizen lab, UMCU, Utrecht, Netherlands. These scripts can be provided on

request. DWI data were analyzed with the FMRIB Diffusion Toolbox. Voxel-wise values of FA and MD were estimated from the original DWI data using “dtifit.”

For alignment of the images to the same space, individual brain images were digitally separated from the triplets in which they were acquired. For the optimal registration of images in GM and WM, two different contrasts were combined (both weighted equally): (i) FA and (ii) and mean of all diffusion weighted directions. A study specific template of all subject images was then acquired using an automated image registration pipeline as described previously (Lerch et al., 2011, 2008). In short, this approach brings all scans into anatomical alignment in an automated and unbiased fashion using a combination of mni_autoreg tools (Collins et al., 1994) and Advanced Normalization Tools (ANTs) (Avants et al., 2008). FSL (for FMRIB Software Library) tools, version 6.0 (www.fmrib.ox.ac.uk/fsl) were used for linear (FLIRT) and nonlinear transformations (FNIRT) to the study specific template (scripts can be provided on request). Transformations gained from this approach were applied to the individual modalities of interest (FA, MD, MTR).

WM structures were analyzed using a modified version of Tract-Based Spatial Statistics (TBSS; Smith et al., 2006). The skeleton for TBSS was thresholded at an FA value of 0.28 as to reliably contain major tracts in the mouse brain that can be accurately aligned across individuals. Finally, the FA values of the tract centers (i.e., maximum FA values) were projected onto the skeleton for each mouse brain and fed into statistical analysis. MD and MTR values for the same voxels were also projected into the skeleton.

4.5.3 | MRI data analysis

For ROI analysis, an aggregate atlas combining 182 individually segmented structures (Dorr et al., 2008; Richards et al., 2011; Steadman et al., 2014; Ullmann et al., 2013) was registered to the unbiased consensus average of the current study the atlas is available at (http://repo.mouseimaging.ca/repo/DSURQE_40micron_nifti) and masks for the specific ROI (M1, M2, S1, Hippocampus) were extracted from the atlas. Mean values from each ROI for each subject were extracted for statistical analysis in R studio. Mixed ANOVAs were used for group comparison, where ROIs were within subject factors and genotype and/or wheel were between subject factors. As data was collected from four consecutive experimental groups, experimental group ($n = 4$) was included as a fixed factor to control for introduced variability. Significant effects in within-subject factor (ROIs) were followed by a post-hoc simple comparison between groups (wheel or genotype), Bonferroni adjusted for number of ROIs. Statistical analysis was performed using R (R Core Team, 2021), using the rstatix package (0.7.2; Kassambara, 2023). To check for outliers, mean values for each metric were extracted from the whole brain mask and checked for extreme outliers (“identify_outliers”, rstatix package, R). One animal (P-Myr^{f^{-/-}}, CW) was identified as an extreme outlier and subsequently removed from the ROI analysis. Statistical analysis including the outlier are provided in Table S2.

For voxel-wise analysis across the whole brain, nonparametric permutation testing with a cluster-forming threshold of $t > 2$ and 5000 permutations were used to determine corrected p values. Clusters with a corrected significance of $p < .05$ were deemed significant. We tested for differences between the genotype groups $Myrf^{(-/-)}$ vs. $Myrf^{(+/-)}$, wheel type (CW vs. FW) and for a genotype \times wheel type interaction (Scripts and GLMs can be provided on request). We also tested for voxel-wise for correlations between contrast and wheel performance (maximum speed, total distance).

Finally, to test for global effects, we calculate mean values for each MR metric across all voxels within the GM mask or the WM skeleton.

4.6 | EEG methods

4.6.1 | Electrophysiology data collection

Chronic electrophysiological recordings were undertaken in seven male adult mice ($P-Myrf^{(-/-)}$: $n = 4$; $P-Myrf^{(+/-)}$: $n = 3$). All mice received tamoxifen at age P75 and were implanted at ages P110–120, and the reported recordings were collected at age P130. The animals were surgically implanted with a custom-made headstage tethered to electrodes for the continuous recording of EEG and electromyogram (EMG). EEG screw electrodes (Fine Science Tools) were inserted into the skull. Five electrodes were implanted in total: above the right and left frontal cortex (primary motor area: anteroposterior +2 mm, mediolateral +2 mm), above the right and left occipital cortex (primary visual area: anteroposterior +3.5 mm, mediolateral +2.5 mm), and above the cerebellum (which served as a reference). As per Fisher et al. (2016) two custom-soldered stainless-steel wires were inserted into the right and left nuchal muscles, respectively, for the recording of EMG. A schematic diagram of implantation locations is shown in Figure 4a.

Immediately before surgery, analgesics were administered (subcutaneous injection of 1–2 mg/kg metacam and 0.08 mg/kg vetergesic). Isoflurane was used for induction and maintenance of anesthesia throughout the surgical procedure (4% and 1%–2%, respectively). After surgery, analgesics were given for at least 3 days (1–2 mg/kg oral metacam) and animal wellbeing was closely monitored for 1–2 weeks, until the animal returned to baseline conditions. All procedures were performed under a UK Home Office Project License and conformed to the Animal Scientific Procedures Act 1986.

Two animals were implanted each day, with all surgeries taking place in the same week. Order of surgery was randomized to ensure balanced allocation of genotype to time of day of surgery (i.e., morning surgery vs. afternoon surgery) and to time of week surgery (i.e., early in the week or late in the week), to avoid systemic bias in implantations and in length of time elapsed between implantation and recording.

4.6.2 | Electrophysiology data processing

Data acquisition were performed using the Multichannel Neurophysiology Recording System (TDT, Alachua FL, USA). EEG/EMG data were filtered between 0.1 and 100 Hz, amplified (PZ5 NeuroDigitizer pre-amplifier, TDT Alachua FL, USA) and stored on a local computer at a sampling rate of 256.9 Hz. EEG/EMG data were resampled offline at a sampling rate of 256 Hz. Signal conversion was performed using custom-written Matlab (The MathWorks Inc, Natick, Massachusetts, USA) scripts and was then transformed into European Data Format (Fisher et al., 2016). Custom MATLAB scripts were used to estimate the power spectral density using the multitaper method (“pmtm()” function, Signal Processing Toolbox, Matlab) for 4-s epochs. A 0.25 Hz resolution was used for plotting of EEG power density across frequency bands. Total power within the 1–30 Hz range across the frontal and occipital channel was calculated and compared using ANOVAs for repeated measures (within-subject factor: location; between subject factor: genotype). Peak frequency was defined as the frequency bin (0.25 Hz resolution) with the highest power. Power within specific frequency bands was calculated and compared between genotype groups: delta, δ (0.5–3 Hz), theta, θ (4–12 Hz), beta, β (12.5–25 Hz), and gamma, γ (30–80 Hz). Statistical analysis was performed using R (R Core Team, 2021), using the rstatix (0.7.0; Kassambara, 2023).

4.6.3 | Scoring and analysis of vigilance states

Recordings were quality-checked during acquisition. All data were manually scored by a blinded investigator (S.R.) for vigilance states, as previously described in Fisher et al. (2016). Briefly, waking was defined based on a low-amplitude fast-frequency EEG activity and high EMG amplitude, NREM sleep was characterized by the predominance of slow waves and sleep spindles on the EEG and low EMG tone, whereas REM sleep was characterized by strong theta EEG activity, especially in the occipital derivation and low EMG activity. To validate scoring accuracy, a subset of the data was re-scored by another investigator (A.L.). Scoring quality was further verified by a third investigator (V.V.). The channel of the left hemisphere was selected for group comparison, unless a blinded investigator (V.V.) indicated that the quality of the data was significantly better in the right hemisphere, in which case the right hemisphere channel was used.

AUTHOR CONTRIBUTIONS

M. S. K., H. J. B. and C. S. B conceived the project and designed the experiments. M. S. K conducted in vivo experiments, analysed the data, constructed figures, wrote the manuscript with input from the co-authors. A. L. and V. V. planned electrophysiology experiments and A. L. conducted surgery and in vivo electrophysiology recording. W. D. R. and T. S. provided the in vivo model and valuable feedback on design and interpretation of the data. D. B. provided valuable



advice on behavioural experiments and interpretation of data. A. v. d. T. scanned and pre-processed ex vivo MRI samples. Y. F. collected behavioural data in wild-type animals. S. R. helped with sleep scoring of electrophysiological data. C. W. T. provided practical help on analysis for electrophysiology. All authors contributed to the article and approved the submitted version.

ACKNOWLEDGMENTS

The work was funded by Wellcome Trust PhD studentships (102393/Z/13/Z) and principal research fellowship (110027/Z/15/Z). The Wellcome Centre for Integrative Neuroimaging is supported by core funding from the Wellcome Trust (203139/Z/16/Z and 203139/A/16/Z). For the purpose of open access, the author has applied a CC BY public copyright license to any Author Accepted Manuscript version arising from this submission. The authors thank Dr. Eveliina Hanski and Dr. Luke Baxter for feedback on previous version of the manuscript. The authors also want to thank Piergiorgio Salva and the entire Plasticity Group at the Wellcome Centre for Integrative Neuroimaging for constructive discussions and suggestions during the project. Table of content graphics created with [BioRender.com](https://www.biorender.com).

CONFLICT OF INTEREST STATEMENT

The authors declare no competing interests.

DATA AVAILABILITY STATEMENT

The data that support the findings of this study are available from the corresponding author upon reasonable request.

ORCID

Malte S. Kaller <https://orcid.org/0000-0002-4904-5037>

Alberto Lazari <https://orcid.org/0000-0002-8688-581X>

Christopher W. Thomas <https://orcid.org/0000-0001-5371-7257>

Takahiro Shimizu <https://orcid.org/0000-0002-8288-5011>

David Bannerman <https://orcid.org/0000-0002-3024-7595>

Vladyslav Vyazovskiy <https://orcid.org/0000-0002-4336-6681>

William D. Richardson <https://orcid.org/0000-0001-7261-2485>

Cassandra Sampaio-Baptista <https://orcid.org/0000-0002-7893-0289>

Heidi Johansen-Berg <https://orcid.org/0000-0002-4134-9730>

REFERENCES

- Avants, B. B., Epstein, C. L., Grossman, M., & Gee, J. C. (2008). Symmetric diffeomorphic image registration with cross-correlation: Evaluating automated labeling of elderly and neurodegenerative brain. *Medical Image Analysis*, 12, 26–41. <https://doi.org/10.1016/j.media.2007.06.004>
- Bacmeister, C. M., Huang, R., Osso, L. A., Thornton, M. A., Conant, L., Chavez, A., Poleg-Polsky, A., & Hughes, E. G. (2022). Motor learning drives dynamic patterns of intermittent myelination on learning-activated axons. *Nature Neuroscience*, 25, 1300–1313. <https://doi.org/10.1101/2021.10.13.464319>
- Bergles, D. E., & Richardson, W. D. (2016). Oligodendrocyte development and plasticity. *Cold Spring Harbor Perspectives in Biology*, 8, a020453. <https://doi.org/10.1101/cshperspect.a020453>
- Bonetto, G., Belin, D., & Káradóttir, R. T. (2021). Myelin: A gatekeeper of activity-dependent circuit plasticity? *Science*, 374, eaba6905. <https://doi.org/10.1126/science.aba6905>
- Collins, D. L., Neelin, P., Peters, T. M., & Evans, A. C. (1994). Automatic 3D intersubject registration of MR volumetric data in standardized Talairach space. *Journal of Computer Assisted Tomography*, 18, 192–205.
- Cullen, C. L., Pepper, R. E., Clutterbuck, M. T., Pitman, K. A., Oorschot, V., Auderset, L., Tang, A. D., Ramm, G., Emery, B., Rodger, J., Jolivet, R. B., & Young, K. M. (2021). Periaxonal and nodal plasticities modulate action potential conduction in the adult mouse brain. *Cell Reports*, 34, 108641. <https://doi.org/10.1016/j.celrep.2020.108641>
- Dawson, M. R. L., Polito, A., Levine, J. M., & Reynolds, R. (2003). NG2-expressing glial progenitor cells: An abundant and widespread population of cycling cells in the adult rat CNS. *Molecular and Cellular Neurosciences*, 24, 476–488. [https://doi.org/10.1016/s1044-7431\(03\)00210-0](https://doi.org/10.1016/s1044-7431(03)00210-0)
- Deloire-Grassin, M. S., Brochet, B., Quesson, B., Delalande, C., Dousset, V., Canioni, P., & Petry, K. G. (2000). In vivo evaluation of remyelination in rat brain by magnetization transfer imaging. *Journal of the Neurological Sciences*, 178, 10–16. [https://doi.org/10.1016/s0022-510x\(00\)00331-2](https://doi.org/10.1016/s0022-510x(00)00331-2)
- Dorr, A. E., Lerch, J. P., Spring, S., Kabani, N., & Henkelman, R. M. (2008). High resolution three-dimensional brain atlas using an average magnetic resonance image of 40 adult C57Bl/6J mice. *NeuroImage*, 42, 60–69. <https://doi.org/10.1016/j.neuroimage.2008.03.037>
- Dubey, M., Pascual-Garcia, M., Helmes, K., Wever, D. D., Hamada, M. S., Kushner, S. A., & Kole, M. H. P. (2022). Myelination synchronizes cortical oscillations by consolidating parvalbumin-mediated phasic inhibition. *eLife*, 11, e73827. <https://doi.org/10.7554/eLife.73827>
- Emery, B., Agalliu, D., Cahoy, J. D., Watkins, T. A., Dugas, J. C., Mulinyawe, S. B., Ibrahim, A., Ligon, K. L., Rowitch, D. H., & Barres, B. A. (2009). Myelin gene regulatory factor is a critical transcriptional regulator required for CNS myelination. *Cell*, 138, 172–185. <https://doi.org/10.1016/j.cell.2009.04.031>
- Fisher, S. P., Cui, N., McKillop, L. E., Gemignani, J., Bannerman, D. M., Oliver, P. L., Peirson, S. N., & Vyazovskiy, V. V. (2016). Stereotypic wheel running decreases cortical activity in mice. *Nature Communications*, 7, 13138. <https://doi.org/10.1038/ncomms13138>
- Foster, A. Y., Bujalka, H., & Emery, B. (2019). Axoglial interactions in myelin plasticity: Evaluating the relationship between neuronal activity and oligodendrocyte dynamics. *Glia*, 67, 2038–2049. <https://doi.org/10.1002/glia.23629>
- Geraghty, A. C., Gibson, E. M., Ghanem, R. A., Greene, J. J., Ocampo, A., Goldstein, A. K., Ni, L., Yang, T., Marton, R. M., Paşca, S. P., Greenberg, M. E., Longo, F. M., & Monje, M. (2019). Loss of adaptive myelination contributes to methotrexate chemotherapy-related cognitive impairment. *Neuron*, 103, 250–265.e8. <https://doi.org/10.1016/j.neuron.2019.04.032>
- Gibson, E. M., Purger, D., Mount, C. W., Goldstein, A. K., Lin, G. L., Wood, L. S., Inema, I., Miller, S. E., Bieri, G., Zuchero, J. B., Barres, B. A., Woo, P. J., Vogel, H., & Monje, M. (2014). Neuronal activity promotes oligodendrogenesis and adaptive myelination in the mammalian brain. *Science*, 344, 1252304. <https://doi.org/10.1126/science.1252304>
- Gould, E. A., Busquet, N., Shepherd, D., Dietz, R. M., Herson, P. S., Simoes de Souza, F. M., Li, A., George, N. M., Restrepo, D., & Macklin, W. B. (2018). Mild myelin disruption elicits early alteration in behavior and proliferation in the subventricular zone. *eLife*, 7, e34783. <https://doi.org/10.7554/eLife.34783>
- Hibbitts, N., Pannu, R., John Wu, T., & Armstrong, R. C. (2009). Cuprizone demyelination of the corpus callosum in mice correlates with altered social interaction and impaired bilateral sensorimotor coordination. *ASN Neuro*, 1, e00013. <https://doi.org/10.1042/AN20090032>

- Hill, R. A., Li, A. M., & Grutzendler, J. (2018). Lifelong cortical myelin plasticity and age-related degeneration in the live mammalian brain. *Nature Neuroscience*, 21, 683–695. <https://doi.org/10.1038/s41593-018-0120-6>
- Hughes, E. G., Orthmann-Murphy, J. L., Langseth, A. J., & Bergles, D. E. (2018). Myelin remodeling through experience-dependent oligodendrogenesis in the adult somatosensory cortex. *Nature Neuroscience*, 21, 696–706. <https://doi.org/10.1038/s41593-018-0121-5>
- Kaller, M. S., Lazari, A., Blanco-Duque, C., Sampaio-Baptista, C., & Johansen-Berg, H. (2017). Myelin plasticity and behaviour-connecting the dots. *Current Opinion in Neurobiology*, 47, 86–92. <https://doi.org/10.1016/j.conb.2017.09.014>
- Kassambara, A. (2023). rstatix: Pipe-Friendly Framework for Basic Statistical Tests. Version 0.7.2.
- Kato, D., Wake, H., Lee, P. R., Tachibana, Y., Ono, R., Sugio, S., Tsuji, Y., Tanaka, Y. H., Tanaka, Y. R., Masamizu, Y., Hira, R., Moorhouse, A. J., Tamamaki, N., Ikenaka, K., Matsukawa, N., Fields, R. D., Nabekura, J., & Matsuzaki, M. (2020). Motor learning requires myelination to reduce asynchrony and spontaneity in neural activity. *Glia*, 68, 193–210. <https://doi.org/10.1002/glia.23713>
- Keiner, S., Niv, F., Neumann, S., Steinbach, T., Schmeer, C., Hornung, K., Schlenker, Y., Förster, M., Witte, O. W., & Redeker, C. (2017). Effect of skilled reaching training and enriched environment on generation of oligodendrocytes in the adult sensorimotor cortex and corpus callosum. *BMC Neuroscience*, 18, 31. <https://doi.org/10.1186/s12868-017-0347-2>
- Knowles, J. K., Batra, A., Xu, H., & Monje, M. (2022). Adaptive and maladaptive myelination in health and disease. *Nature Reviews. Neurology*, 18, 735–746. <https://doi.org/10.1038/s41582-022-00737-3>
- Lakhani, B., Borich, M. R., Jackson, J. N., Wadden, K. P., Peters, S., Villamayor, A., MacKay, A. L., Vavasour, I. M., Rauscher, A., & Boyd, L. A. (2016). Motor skill acquisition promotes human brain myelin plasticity. *Neural Plasticity*, 2016, 7526135. <https://doi.org/10.1155/2016/7526135>
- Lazari, A., & Lipp, I. (2021). Can MRI measure myelin? Systematic review, qualitative assessment, and meta-analysis of studies validating microstructural imaging with myelin histology. *NeuroImage*, 230, 117744. <https://doi.org/10.1016/j.neuroimage.2021.117744>
- Lerch, J. P., Carroll, J. B., Dorr, A., Spring, S., Evans, A. C., Hayden, M. R., Sled, J. G., Henkelman, R. M. (2008). Cortical thickness measured from MRI in the YAC128 mouse model of Huntington's disease. *NeuroImage*, 41, 243–251.
- Lerch, J. P., Yiu, A. P., Martinez-Canabal, A., Pekar, T., Bohbot, V. D., Frankland, P. W., Henkelman, R. M., Josselyn, S. A., Sled, J. G. (2011). Maze training in mice induces MRI-detectable brain shape changes specific to the type of learning. *NeuroImage*, 54, 2086–2095.
- Liebetanz, D., Baier, P. C., Paulus, W., Meuer, K., Bähr, M., & Weishaupt, J. H. (2007). A highly sensitive automated complex running wheel test to detect latent motor deficits in the mouse MPTP model of Parkinson's disease. *Experimental Neurology*, 205, 207–213. <https://doi.org/10.1016/j.expneurol.2007.01.030>
- McKenzie, I. A., Ohayon, D., Li, H., de Faria, J. P., Emery, B., Tohyama, K., & Richardson, W. D. (2014). Motor skill learning requires active central myelination. *Science*, 346, 318–322. <https://doi.org/10.1126/science.1254960>
- Mitew, S., Gobijs, I., Fenlon, L. R., McDougall, S. J., Hawkes, D., Xing, Y. L., Bujalka, H., Gundlach, A. L., Richards, L. J., Kilpatrick, T. J., Merson, T. D., & Emery, B. (2018). Pharmacogenetic stimulation of neuronal activity increases myelination in an axon-specific manner. *Nature Communications*, 9, 306. <https://doi.org/10.1038/s41467-017-02719-2>
- Nave, K.-A. (2010). Myelination and support of axonal integrity by glia. *Nature*, 468, 244–252. <https://doi.org/10.1038/nature09614>
- Noori, R., Park, D., Griffiths, J. D., Bells, S., Frankland, P. W., Mabbott, D., & Lefebvre, J. (2020). Activity-dependent myelination: A glial mechanism of oscillatory self-organization in large-scale brain networks. *Proceedings of the National Academy of Sciences*, 117, 13227–13237. <https://doi.org/10.1073/pnas.1916646117>
- Pajevic, S., Basser, P. J., & Fields, R. D. (2014). Role of myelin plasticity in oscillations and synchrony of neuronal activity. *Neuroscience*, 276, 135–147. <https://doi.org/10.1016/j.neuroscience.2013.11.007>
- Pajevic, S., Plenz, D., Basser, P. J., & Fields, R. D. (2023). Oligodendrocyte-mediated myelin plasticity and its role in neural synchronization. *eLife*, 12, e81982. <https://doi.org/10.7554/eLife.81982>
- Pan, S., Mayoral, S. R., Choi, H. S., Chan, J. R., & Kheirbek, M. A. (2020). Preservation of a remote fear memory requires new myelin formation. *Nature Neuroscience*, 23, 487–499. <https://doi.org/10.1038/s41593-019-0582-1>
- R Core Team (2021). R: A language and environment for statistical computing. *R Foundation for Statistical Computing*, Vienna, Austria. <https://www.R-project.org/>
- Richards, K., Watson, C., Buckley, R. F., Kurniawan, N. D., Yang, Z., Keller, M. D., Beare, R., Bartlett, P. F., Egan, G. F., Galloway, G. J., Paxinos, G., Petrou, S., & Reutens, D. C. (2011). Segmentation of the mouse hippocampal formation in magnetic resonance images. *NeuroImage*, 58, 732–740. <https://doi.org/10.1016/j.neuroimage.2011.06.025>
- Rivers, L. E., Young, K. M., Rizzi, M., Jamen, F., Psachoulia, K., Wade, A., Kessaris, N., & Richardson, W. D. (2008). PDGFRA/NG2 glia generate myelinating oligodendrocytes and piriform projection neurons in adult mice. *Nature Neuroscience*, 11, 1392–1401. <https://doi.org/10.1038/nn.2220>
- Salzer, J. L., & Zalc, B. (2016). Myelination. *Current Biology*, 26, R971–R975. <https://doi.org/10.1016/j.cub.2016.07.074>
- Sampaio-Baptista, C., & Johansen-Berg, H. (2017). White matter plasticity in the adult brain. *Neuron*, 96, 1239–1251. <https://doi.org/10.1016/j.neuron.2017.11.026>
- Sampaio-Baptista, C., Khrapitchev, A. A., Foxley, S., Schlagheck, T., Scholz, J., Jbabdi, S., DeLuca, G. C., Miller, K. L., Taylor, A., Thomas, N., Kleim, J., Sibson, N. R., Bannerman, D., & Johansen-Berg, H. (2013). Motor skill learning induces changes in white matter microstructure and myelination. *Journal of Neuroscience: The Official Journal of the Society for Neuroscience*, 33, 19499–19503. <https://doi.org/10.1523/JNEUROSCI.3048-13.2013>
- Sampaio-Baptista, C., Vallès, A., Khrapitchev, A. A., Akkermans, G., Winkler, A. M., Foxley, S., Sibson, N. R., Roberts, M., Miller, K., Diamond, M. E., Martens, G. J. M., de Weerd, P., & Johansen-Berg, H. (2020). White matter structure and myelin-related gene expression alterations with experience in adult rats. *Progress in Neurobiology*, 187, 101770. <https://doi.org/10.1016/j.pneurobio.2020.101770>
- Schalomon, P. M., & Wahlsten, D. (2002). Wheel running behavior is impaired by both surgical section and genetic absence of the mouse corpus callosum. *Brain Research Bulletin*, 57, 27–33. [https://doi.org/10.1016/S0361-9230\(01\)00633-5](https://doi.org/10.1016/S0361-9230(01)00633-5)
- Scholz, J., Klein, M. C., Behrens, T. E. J., & Johansen-Berg, H. (2009). Training induces changes in white-matter architecture. *Nature Neuroscience*, 12, 1370–1371. <https://doi.org/10.1038/nn.2412>
- Shimizu, T., Nayar, S. G., Swire, M., Jiang, Y., Grist, M., Kaller, M., Sampaio Baptista, C., Bannerman, D. M., Johansen-Berg, H., Ogasawara, K., Tohyama, K., Li, H., & Richardson, W. D. (2023). Oligodendrocyte dynamics dictate cognitive performance outcomes of working memory training in mice. *Nature Communications*, 14, 6499. <https://doi.org/10.1038/s41467-023-42293-4>
- Smith, S. M., Jenkinson, M., Johansen-Berg, H., Rueckert, D., Nichols, T. E., Mackay, C. E., Watkins, K. E., Ciccarelli, O., Cader, M. Z., Matthews, P. M., & Behrens, T. E. J. (2006). Tract-based spatial statistics: Voxelwise analysis of multi-subject diffusion data. *NeuroImage*, 31, 1487–1505. <https://doi.org/10.1016/j.neuroimage.2006.02.024>
- Srinivas, S., Watanabe, T., Lin, C.-S., William, C. M., Tanabe, Y., Jessell, T. M., & Costantini, F. (2001). Cre reporter strains produced by targeted insertion of EYFP and ECFP into the ROSA26 locus. *BMC Developmental Biology*, 1, 4. <https://doi.org/10.1186/1471-213X-1-4>



- Steadman, P. E., Ellegood, J., Szulc, K. U., Turnbull, D. H., Joyner, A. L., Henkelman, R. M., & Lerch, J. P. (2014). Genetic effects on cerebellar structure across mouse models of autism using a magnetic resonance imaging atlas. *Autism Research*, 7, 124–137. <https://doi.org/10.1002/aur.1344>
- Steadman, P. E., Xia, F., Ahmed, M., Mocle, A. J., Penning, A. R. A., Geraghty, A. C., Steenland, H. W., Monje, M., Josselyn, S. A., & Frankland, P. W. (2020). Disruption of Oligodendrogenesis impairs memory consolidation in adult mice. *Neuron*, 105, 150–164.e6. <https://doi.org/10.1016/j.neuron.2019.10.013>
- Talidou, A., Frankland, P. W., Mabbott, D., & Lefebvre, J. (2022). Homeostatic coordination and up-regulation of neural activity by activity-dependent myelination. *Nature Computational Science*, 1–12, 665–676. <https://doi.org/10.1038/s43588-022-00315-z>
- Ullmann, J. F. P., Watson, C., Janke, A. L., Kurniawan, N. D., & Reutens, D. C. (2013). A segmentation protocol and MRI atlas of the C57BL/6J mouse neocortex. *NeuroImage*, 78, 196–203. <https://doi.org/10.1016/j.neuroimage.2013.04.008>
- Xiao, L., Ohayon, D., McKenzie, I. A., Sinclair-Wilson, A., Wright, J. L., Fudge, A. D., Emery, B., Li, H., & Richardson, W. D. (2016). Rapid production of new oligodendrocytes is required in the earliest stages of motor-skill learning. *Nature Neuroscience*, 19, 1210–1217. <https://doi.org/10.1038/nn.4351>
- Xin, W., & Chan, J. R. (2020). Myelin plasticity: Sculpting circuits in learning and memory. *Nature Reviews. Neuroscience*, 21, 682–694. <https://doi.org/10.1038/s41583-020-00379-8>
- Young, K. M., Psachoulia, K., Tripathi, R. B., Dunn, S.-J., Cossell, L., Attwell, D., Tohyama, K., & Richardson, W. D. (2013). Oligodendrocyte dynamics in the healthy adult CNS: Evidence for myelin remodeling. *Neuron*, 77, 873–885. <https://doi.org/10.1016/j.neuron.2013.01.006>
- Zatorre, R. J., Fields, R. D., & Johansen-Berg, H. (2012). Plasticity in gray and white: Neuroimaging changes in brain structure during learning. *Nature Neuroscience*, 15, 528–536. <https://doi.org/10.1038/nn.3045>

SUPPORTING INFORMATION

Additional supporting information can be found online in the Supporting Information section at the end of this article.

How to cite this article: Kaller, M. S., Lazari, A., Feng, Y., van der Toorn, A., Rühling, S., Thomas, C. W., Shimizu, T., Bannerman, D., Vyazovskiy, V., Richardson, W. D., Sampaio-Baptista, C., & Johansen-Berg, H. (2024). Ablation of oligodendrogenesis in adult mice alters brain microstructure and activity independently of behavioral deficits. *Glia*, 1–18. <https://doi.org/10.1002/glia.24576>